Title: An Internal Crown Geometric Model for Conifer Species Classification With High-Density LiDAR Data

This paper appears in: IEEE Transactions on Geoscience and Remote Sensing

Date of Publication: 16 February 2017

Author(s): Aravind Harikumar ; Francesca Bovolo ; Lorenzo Bruzzone

Volume: 55 , Issue: 5

Page(s): 2924 - 2940

DOI: 10.1109/TGRS.2017.2656152

An Internal Crown Geometric Model for Conifer Species Classification with High Density LiDAR Data

Aravind Harikumar, *Student Member, IEEE,* Francesca Bovolo, *Senior Member, IEEE,* and Lorenzo Bruzzone, *Fellow, IEEE*

***Abstract*—The knowledge of the tree species is a crucial information that governs the success of precision forest management practice. High density small footprint multi-return airborne Light Detection and Ranging (LiDAR) scanning can collect a huge amount of point samples containing structural details of the forest vertical profile, which can reveal important structural information of the forest components. LiDAR data have been successfully used to distinguish between coniferous and deciduous/broadleaved tree species. However species classification within a class (e.g., the conifer class) using LiDAR data is a challenging problem when considering the tree external crown characteristics only. This paper presents a novel method for conifer species classification based on the use of geometric features describing both the internal and external structure of the crown. The Internal Crown Geometric Features (IGFs) are defined based on a novel internal branch structure model which uses 3D region growing and Principal Component Analysis (PCA) to delineate the branch structure of a conifer tree accurately. Internal crown geometric features are used together with external crown geometric features (EGFs) to perform conifer species classification. Three different Support Vector Machines (SVM) have been considered for classification performance evaluation. The experimental analysis conducted on high density LiDAR data acquired over a portion of the Trentino region in Italy proves the effectiveness of the proposed method.**

***Index Terms*—Conifers, Tree Species, Feature Extraction, Support Vector Machines (SVM), Airborne Laser Scanning, Light Detection and Ranging (LiDAR), Forestry.**

I. INTRODUCTION

FORESTS are an extremely important natural resource and need to be preserved for obvious environmental and economic reasons. An efficient forest management and planning is essential for effective forest preservation [1]. However such planning demands an accurate and periodic collection of forest inventory data like tree height, stem diameter at breast height, canopy density, crown cover, and biomass at individual tree level. Most of the above mentioned parameters are species specific. Thus the knowledge about tree species is fundamental for activities such as forest ecological studies, biodiversity studies [2], and climate change studies [3].

Conventional forest inventory methods require huge efforts in terms of time and costs, whereas it is widely assessed that remote sensing technologies allow a reduction of both the amount of human intervention for data collection [4] and the overall cost. Light Detection and Ranging (LiDAR) is one of the most effective and widely used remote sensing technology for acquiring data about forest structure [5], [6]. Airborne Laser Scanning (ALS) acquisitions conducted with the help of Global Positioning System (GPS) and Inertial Navigation System (INS) make it possible to obtain very accurate three-dimensional (3D) measures of forest structure. However, traditional LiDAR systems with relatively low laser sampling rate (and thus low sample density) are often not good enough for estimating biophysical parameters with sufficient accuracy. Accordingly, such low density airborne LiDAR data are often used for tree species classification together with information provided by other sources such as optical remote imaging sensors [7]. However, recent improvements in sampling rate of small footprint airborne LiDAR systems allow to sample laser returns at a finer time interval over a smaller field-of-view (FOV). As a result, they capture multiple returns from a small area (i.e., 0.2 - 1.2m^2), and thus ensure the availability of a higher number of data points per unit area (i.e., high density). These kind of LiDAR systems are optimal for studying forests at the single tree level. Modern small footprint multi-return airborne LiDAR scanners, such as Leica ALS80 and RIEGL LMS-Q680i, can produce dense point clouds. For example, in multi-return mode, Leica ALS80 can record more than 50 samples/m^2 in a single scanning pass conducted from a height of about 1km and at a ground speed of 100 km/h. Hence data acquired by these systems contain a large amount of information on both the tree crown characteristics and the branch characteristics within the crown. The large amount of spatial information obtained by small footprint high point density multi-return airborne LiDAR scanners over forest areas allows to perform an accurate classification of tree species [8] and to better estimate parameters such as tree height, crown area, and biomass [5]. Such LiDAR systems also record the intensity of the laser return along with its time of reception. The intensity information is also useful for studying the spectral characteristics of trees, and thus is often beneficial for species classification [9], [10].

Many algorithms have been developed for individual tree delineation and biophysical parameters estimation from LiDAR data only. Some of them take advantage of combining information in LiDAR data with the ones obtained from complementary data sources such as Hyperspectral [11], Mul-

Aravind Harikumar and Lorenzo Bruzzone are with the Department of Information Engineering and Computer science, Trento, Italy. E-mail: (see aravind.harikumar@unitn.it).

Aravind Harikumar and Francesca Bovolo are with Fondazione Bruno Kessler, Trento, Italy.

Manuscript received March 1, 2016

tispectral [12], Very High Geometrical Resolution (VHR)[13], and Synthetic Aperture Radar (SAR) images [14]. However, using multi-sensor data is complex, often costly and sometimes impossible. For example, one has to consider the need for accurate multi-source data coregistration in that case. Hence, it becomes interesting to optimize information extraction techniques that can work with data acquired by a single sensor such as the high resolution airborne LiDAR. Although, data acquired from multispectral/hyperspectral sensors are useful for generating good spectral signatures based models, they show poor capability in modelling the 3D structure of forest. Among the single sensor based species classification studies in the literature, several uses high density LiDAR data [9], [10]. This is due to the recent realization on the importance of the crown structure (both internal and external) for accurate species classification [15], [10]. However, methods for identifying the species of a tree belonging to the same taxonomic class (e.g., conifers) are lacking. Accordingly, here we focus on developing an effective technique for extracting crown structural information using small footprint high point density multi-return airborne LiDAR data.

In this paper, considering the fact that conifers are very important from an ecological point of view and dominate the European forests, we introduce a novel method that utilizes the structural/geometric information present in small footprint high point density multi-return airborne LiDAR data for identifying the species of trees belonging to the conifer class (i.e., Pinopsida). Conifer species classification using LiDAR data is challenging due to the high similarity in their external crown shape (i.e., the external crown characteristics). Concerning the internal crown characteristics (i.e., the branch structure inside crown), conifers have a linear main stem with branches growing outward from the stem, in an approximately linear fashion, almost perpendicular to the stem. The separation between conifer branches increases as we move from the stem toward the external part of the crown. This makes the branches more distinguishable near the exterior of the tree crown (see Fig. 1). However, each conifer species shows specific stem/branch attributes that makes it different from the others. Accordingly, the objectives of this paper are: (1) to develop a robust method to model the internal structure of a coniferous tree from the LiDAR data; (2) to define robust, efficient and scale invariant geometric features representing the branch level characteristics of conifers based on the proposed internal crown structure model; (3) to demonstrate the relevance of internal crown geometric features; and (4) to perform effective conifer species classification. Experimental analysis was conducted on a LiDAR dataset acquired by an airborne high density LiDAR system by conducting multiple passes over a study area located in the north west part of the Trentino region in Italy. Validation was concentrated on four major European conifer species, i.e., the Norway Spruce (NS), the European Larch (EL), the Swiss Pine (SP) and the Silver Fir (SF). However, the method can be extended to the classification of other conifer species. In our experiments, linear Sparse C-SVM, non-linear C-SVM, and non-linear multi-kernel C-SVM (MK C-SVM) classifiers were used. Linear Sparse C-SVM is used for feature relevance analysis. This is because linear Sparse C-SVM has the capability to assign larger weights (i.e., hyperplane parameters) for relevant features, while smaller weights are assigned to the remaining features. Accuracy assessment was conducted by comparing classification results achieved by the three above mentioned classifiers. The rest of the paper is organized as follows. Section II presents the state-of-the-art techniques for tree species classification using LiDAR data. Section III describes the proposed method to model the internal branch structure and briefly illustrates the theory of SVM classifiers involved in the experiments. Section IV introduces the dataset and the study area, and provides experimental results. Section V draws the conclusion of this work.

II. Tree-species Classification with LiDAR Data

Obtaining tree species information from small footprint single-return low sampling rate (i.e., low point density) airborne LiDAR systems is difficult due to their inability to capture enough samples from the interior of trees. In remote sensing based forest survey, the availability of small footprint high sampling rate multi-return airborne (i.e., high point density) LiDAR data is a major achievement which has the potential to trigger a paradigm shift in the inventorying approach, from the stand based [16] to the individual tree based one [8], [17]. The latter is particularly advantageous for studying forests in detail, as it allows to obtain detailed information on the crown structure, the height, the diameter at breast height and the biomass of individual trees. However, algorithms working at the individual tree level require that the LiDAR data corresponding to individual tree crowns are accurately delineated prior to providing them to the species classification algorithm.

In the case of fully automatic species classification and biophysical parameter estimation techniques, the efficiency in individual tree crown delineation is very critical for any downstream processing. Initial success in individual tree crown detection was achieved using segmentation of Landsat-TM (optical) data [18]. However, segmentation conducted on high resolution airborne optical sensors [19], [20] and Very High Resolution (VHR) satellite borne optical sensors [21] were found to provide more accurate results. Attempts to delineate trees using LiDAR data proved to be relatively more successful than using optical data, as LiDAR data contain information about the vertical profile of forests, while optical data provide only the 2D canopy level information. Several methods [22], [23], [24] that use LiDAR data only for individual tree crown delineation also exist in the literature, and most of them provide a relatively better performance than optical data. The underlying assumption while using LiDAR data is that the local maxima in Canopy Height Model (CHM) [5] correspond to tree-tops. Delineation of individual tree crowns from CHM is achieved in LiDAR data by applying algorithms such as active contour [5], watershed segmentation [25], and region growing [22]. Alternatively, Falkowski, et al. [26] used two-dimensional (2D) spatial-wavelet analysis to detect individual tree crowns and estimate their crown diameter in a mixed conifer forest. Low density LiDAR data have been found

(a) (b) (c) (d)

Fig. 1: Examples of the four different coniferous species considered in the study; (a) Norway spruce (Picea abies), (b) European larch (Larix decidua), (c) Swiss pine (Pinus cembra), and (d) Silver fir (Abies alba).

reliable only in the case of simple forests with little or no undergrowth, while, with high density LiDAR data much better accuracies were reported in tree crown delineation [24], [8]. In [27], a hierarchical approach to 3D segmentation of multilayered forests is provided that delineates both dominant and sub-dominant trees very accurately for a study area in Trentino, Italy. However, undergrowth is still a problem with most single tree delineation algorithms [17], [28]. In [29] and [30] it is demonstrated that improvements in tree detection can be achieved by jointly exploiting the complementary information of passive imaging sensors and high density LiDAR data. However, practical issues such as unavailability of multi-sensor data, increased multi-sensor data acquisition and processing (e.g., data coregistration) complexity are often a problem.

Once the data corresponding to individual trees are delineated, any of the several algorithms in the literature can be used for tree species classification depending on the data-type (e.g., VHR optical images, LiDAR data). Many attempts have been performed for tree species classification with optical remote sensing images by extracting branch structure [31] and external crown shape features [32]. Törmä [33] was among the first ones to test the usability of low point density small footprint airborne LiDAR data for deriving species proportions in forest stands by using features that characterize the vertical distribution of the laser measurements. However, the study reports a low classification performance. Later researchers investigated the effectiveness of multi-return LiDAR data for species classification. For example, Pyysalo and Hyyppä [25] proved that the profile of distance of LiDAR points from the stem along the vertical direction provides hints on the tree species. In [34], the height difference between the first and last pulse from a small footprint high sampling rate multi-return LiDAR system has been identified as a good feature for differentiating deciduous trees from conifers during leaf-off conditions. The underlying assumption here is that the last laser return is reflected from within the deciduous tree crown, while the same would get reflected back from crown-top in case of conifers. The small footprint high sampling-rate multi-return LiDAR systems collect a large number of high resolution samples per square meter, thus improving the possibility of performing accurate species classification by acquiring fine structural details of forest components. Holmgren [35] extracted information such as the spatial distribution of point samples, an approximate external crown geometry, and the return intensity, from a high density LiDAR point cloud, to discriminate between pine and spruce, obtaining an accuracy of 95.0%. The possibility of using LiDAR intensity data and crown-structure features in differentiating conifers from broadleaved has been analyzed in [36], where combining leaf-off and leaf-on data provided accurate results. Even though the technique is able to exploit the variations in annual spectral reflectance of trees for increasing species classification accuracy, it requires data acquisition in two seasons, resulting in high operational costs.

Despite the fact that multi-sensor data assimilation is a costly and complex affair, some researchers studied the effect of combining complementary information for an accurate forest inventory. High resolution Near-infrared (NIR) images have been identified as a valuable source of complementary information for improving the performance of LiDAR based conifer-deciduous classification [37]. Some authors [21], [38] studied the use of high resolution multispectral images to derive species specific details. However, the low spectral resolution of these data is a bottleneck for an efficient species classification. Instead, the fine spectral sampling achieved by hyperspectral sensors enables the discrimination of several species but at a lower spatial resolution. Hyperspectral data have been used in several studies alongside airborne LiDAR data [11], [29]. Sugumaran et al. used LiDAR and hyperspectral data jointly for tree species classification in urban scenarios [39]. In [14], the effectiveness of combining data from LiDAR, SAR, Landsat ETM+, and Quickbird data for forest parameter estimation was investigated. Their joint use was found to be more effective than using LiDAR data only. However, the same study points out that LiDAR is the best single sensor for estimating the canopy height and the biomass of trees with good accuracy. This understanding was a motivation for many studies [36], [30], [15] on species classification using only LiDAR data.

Holmgren et al. distinguished Norway spruce from Scots pine (both conifers) using small footprint high point density airborne LiDAR data and features derived from laser return proportions and point height distributions. They achieved an overall accuracy of 95.0% [35] for Remningstorp area located in Sweden. However, the authors state lack of confidence in obtaining such accuracy in other areas. Kim et al. showed that height percentile value and features derived from fitting simple geometric shapes such as cylinder, cone and sphere, on the tree crown are very useful for classifying deciduous and evergreen trees [36]. However, the use of leaf-off and leaf-on data increases computational complexity and operational cost [9]. In [15], Ko et al. pointed out the importance of internal crown geometric features derived from LiDAR to perform tree species classification. They derived six geometric features from a small footprint high point density multi-return airborne LiDAR data, including two internal and four external ones, for species classification. The classification of pine (coniferous), poplar (coniferous) and maple (broad-leaved) trees achieved an overall accuracy close to 90.0%. Whatsoever, it is worth noting that the study reports low classification accuracies within the conifer class. This is because the Merge and Split K-means based model used in the study is not able to accurately model the individual conifer branch clusters and hence produces unreliable feature values, ultimately leading to poor classification performance. In [10], the authors have demonstrated that point-space distribution, laser return intensity, and internal and external tree geometric features are effective in boreal tree species classification. Concerning classification tools, most studies on tree species classification agree that Support Vector Machines (SVM) are highly effective classification technique for LiDAR data [11], [40].

III. Conifer Species Crown Structure Characterization and Classification

Here, we propose an effective method for conifer species classification based on the structural properties of conifers derived from small footprint high point density multi-return airborne LiDAR data. The approach assumes that the LiDAR point clouds corresponding to individual conifer trees have been isolated (see example in Fig. 3(a)). Any method available in the literature (e.g., [23], [41], [27]) can be employed to this purpose. Starting from the individual tree LiDAR point cloud, two sets of crown geometric features are derived that describe the tree crown from two complementary perspectives: i) the external one; and ii) the internal one. The former set includes six External Crown Geometric Features (EGFs) that capture the external behaviours of crown structural characteristic of conifers. The latter set includes six novel Internal Crown Geometric Features (IGFs) that model the internal behaviour of conifers crown. This is achieved by exploiting the branch structure. The twelve features are used for conifer species classification. In our experiments SVM has been employed to this end with different kernels and architectures [42], [43]. The block scheme of the proposed approach is given in Fig. 2.

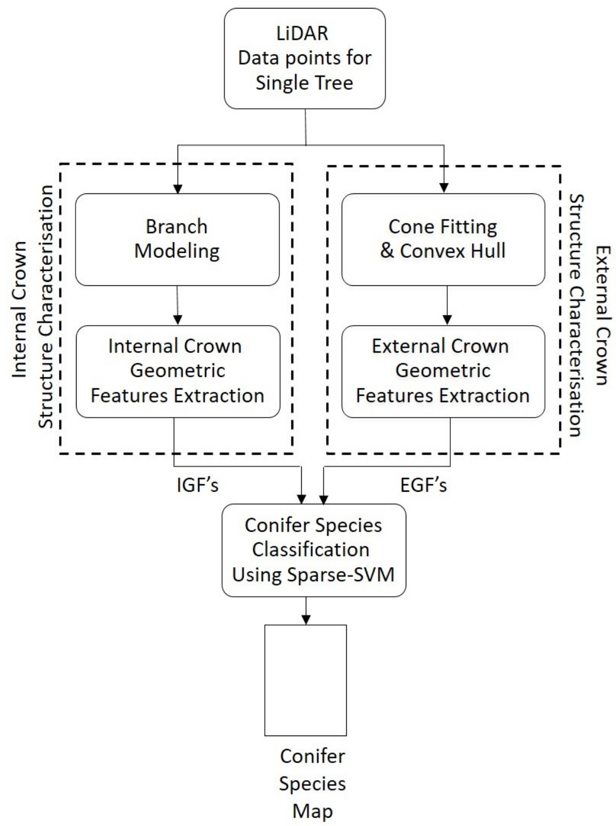

Fig. 2: Block scheme of the proposed approach to conifer species classification.

A. Internal Crown Structure Characterization

In order to properly model the internal crown structure of conifers crown, let us observe that: i) conifers have a linear/vertical central stem; ii) branches grow from the stem outward; and iii) branches are linear and compact and have a direction which is almost perpendicular to the stem and reach the maximum distance from each other at branch tips. The internal crown structural characteristics of conifers can be defined by studying their branch characteristics such as the branch length, the branch symmetry and the branch density. Thus, individual branches of conifers need to be identified.

We have assumed the following notations to describe LiDAR data at the tree level. Let $P = \{p_1, p_2 \ldots, p_N\}$ be the LiDAR point cloud representing a single tree, where $p_n \in P$ is the spatial position of each point belonging to the tree in the small footprint high density multi-return LiDAR cloud. p_n is fully described in a 3D Euclidean feature space by its

x_n, y_n and z_n Cartesian coordinates. Let M_T be the central stem and B the total number of branches that constitutes the conifer skeleton. In the LiDAR point cloud of a singel tree, each branch can be modeled as a cluster of points (referred to as branch cluster) $c_b = \{p_n; n \in I_b\}$, where I_b is the index set of all the LiDAR points belonging to c_b. The set $C = \{c_b, b \in [1, B]\}$ of B branch clusters obtained by grouping LiDAR points in P represents the entire conifer tree crown. It is worth noting that the laser sampling can be non uniform from the spatial point of view (thus different trees may show a large difference in the numbers of LiDAR samples) and that the number of reflections is relatively large near the external part of the tree crown and relatively smaller towards its interior (i.e., near the stem).

Considering these properties, we developed a conifer branch modelling technique that applies 3D region growing [44] to the data and identifies LiDAR points associated with each branch. However, the accuracy of region growing (and in-turn the accuracy of the internal crown structural model), highly depends on the seed point initialization. Here, we consider the LiDAR points most proximal to the actual conifer branch tips as the optimal seed points for three reasons: 1) the structural properties of conifer branches (i.e., compact and having tapering tips) allow an accurate identification of branch tips in high density LiDAR data; 2) conifers branch tips are prominent in high density LiDAR point cloud; 3) maximum separation between branches occurs at the branch tip (i.e., near the exterior of the crown), and this ensures that the seed points are uniformly separated or at least not confusingly close to each other. We refer to the region growing seed points as the branch tip points.

In case of conifers, it is highly likely that the boundary points of LiDAR point cloud are also the branch tip points. In this paper, branch tip detection is achieved by the boundary detection algorithms in [45]. The algorithm finds the indices of those LiDAR points which define the smallest surface enveloping the entire point cloud. The compactness of the surface is controlled by a variance parameter that can take values between 0 and 1. When the parameter is set to 0, the surface becomes the least compact, and the surface becomes the most compact when the parameter is set to 1. Due to high density of LiDAR points, often multiple points near the same branch tips are selected as boundary points. However, only the most distant point (among the multiple boundary points) from the stem is considered as the optimal branch tip point. The space spanned by the candidate boundary points is dependent on the species. Moreover, the branch width/size varies along the height of the tree, i.e., the lower branches are larger and wider than the branches near the tree top. Hence we use an adaptive thresholding calculated using an inverse linear function of the branch tip point value z_i. The adaptive threshold takes into account also the variation in branch width/size along the height of the tree, i.e., the lower branches are larger and wider than the branches near the tree top. A convex hull formed from the boundary points is shown in Fig. 3b, and the boundary points after thresholding are shown in Fig. 3c.

The branch tips obtained using [45] are the most external LiDAR points in every branch cluster. To define branches, a region growing is performed by progressively grouping LiDAR points, seeding from the identified branch tip points, according to a proximity criterion in the Euclidean space. The proximity calculation is performed on a four dimensional vector including the spatial coordinates of the LiDAR points, and the neighbourhood point density S_n. The neighbourhood point density S_n of the n^{th} LiDAR point sample p_n and can be calculated for each LiDAR point as:

$$S_n = \frac{Y_B}{\sum_{i=0}^{K} D_{ni}} \tag{1}$$

where Y_B is the number of nearest neighbours (a constant) of the n^{th} LiDAR point $p_n \in P$, and D_{ni} is the Euclidean distance between the n^{th} and the i^{th} LiDAR point. Thus, S_n will be large for those points which have close neighbours and viceversa. However, the LiDAR point density becomes considerably low towards the interior of the tree [24], [17], and as a result the inter-point distance (i.e., D_{ni}) becomes large, resulting in low S_n value. In effect, the closer to the stem, the more unreliable is the 3D region growing procedure. Hence, the growth process is stopped when the inter-point density difference becomes larger than a certain threshold. This threshold has been derived empirically by experimental analysis accomplished on a large set of conifers. Thus, samples close to the stem are not assigned to any branch cluster yet. Branch clusters with small number of points (i.e., < 10 points) were found to provide unrealistic branches and hence are not modeled. Such branch clusters mainly occur near the tree tops (due to small branch length) and also near the bottom (due to low point density).

Each incomplete branch cluster is usually highly correlated and linear in the 3D Eucleadian space. This is evident since its overall shape can be approximated with a highly oblige ellipsoid (see Fig. 5). Accordingly, the geometrical properties of individual branches can be approximated to the ones of the ellipsoid. To estimate the parameters of the b^{th} ellipsoid, Principal Component Analysis (PCA) is applied to the LiDAR points of branch clusters $c_b, b = [1, \ldots, B]$ (e.g., see yellow points in Fig. 5) thus obtaining three principal components (PCs). PC1 is the axis along which data show the maximum variance and thus it is usually directed towards the stem of the tree. The angle between PC1 and the stem corresponds to the slope of the branch. PC2 and PC3 (i.e., the second and third largest variance components) provide information about the branch's horizontal and vertical width. Eigenvalues λ_1^b, λ_2^b and λ_3^b associated with the three PCA axis represent the ellipsoidal dimensions and thus the branch cluster dimensions. For each branch cluster, a regression line can be fitted in the 3D Euclidean space, which closely represents the wooden part of the branch. We refer to this as the branch line and it gives an approximate direction of the branch. For the purpose of cluster completion, all the points near the stem that were not allocated previously, are now assigned to one of the B branch clusters based on the proximity of the point to the branch line. Such points are very small in number and do not have much influence on the branch parameters.

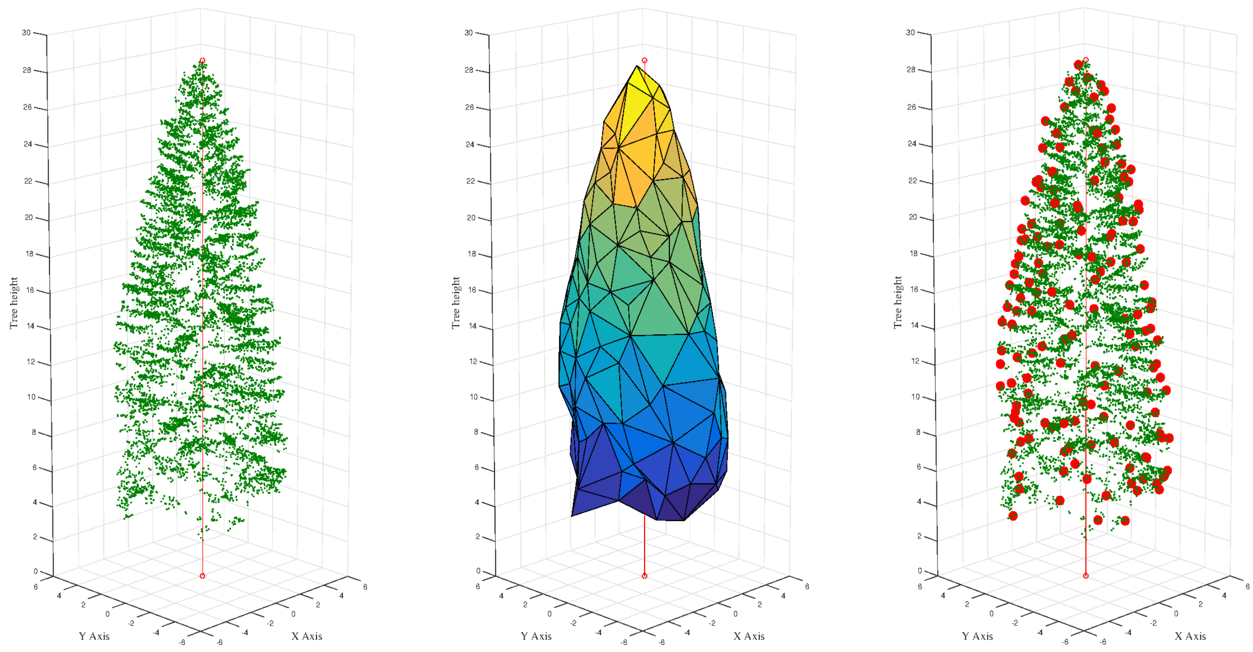

(a) (b) (c)

Fig. 3: Internal crown structure modelling of conifers. (a) Input LiDAR point cloud for a tree (green dots). (b) The convex hull formed on the cloud. (c) Detected branch tips points (red dots).

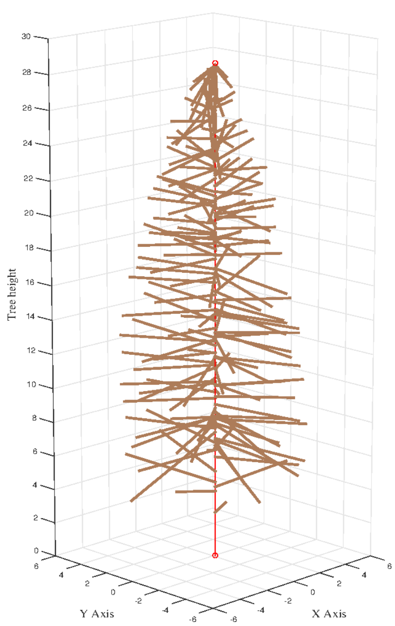

Fig. 4: Conifer branch skeleton

The branch lines together with the stem provide a representation of the internal crown structure of a conifer (i.e., the conifer skeleton) (see Fig. 4). Accordingly, the skeleton can be used to extract Internal Crown Geometrical Features (IGFs) that model the tree branch structure and are useful in distinguishing species.

Here, we define a set of six IGFs at tree level that depends on six corresponding branch-level features that derive from the proposed internal crown model. The set of branch-level features is as follows:

(a) *Branch length* L_b: distance between the b^{th} branch tip and the tree stem computed along the direction of its respective PC1.
(b) *Branch slope* α_b: angle between the direction of the PC1 of the b^{th} branch cluster and the stem.
(c) *Branch compactness* K_b: average of the perpendicular distance of LiDAR points in the branch to the corresponding branch line.
(d) *Branch width* W_b calculated as the Eigenvalue along PC2 i.e., λ_2^b.
(e) *Branch symmetry* S_b: ratio between eigenvalues λ_2^b and λ_3^b. If the value is 1, the symmetry of the branch is considered to be maximum, whereas when the value tends to ∞ (i.e., $\lambda_2^b >> \lambda_3^b$) the branch is considered to be completely asymmetric or flat.
(f) *Branch density* D_b: number of LiDAR points associated with the b^{th} branch cluster c_b. Although, the feature does not capture the actual branch density, the feature value is directly correlated to the actual branch density.

The six IGFs are calculated for each branch and a feature-wise averaging is performed, thus obtaining values of the six features at the tree level. These features form half the number of feature that are given as input to the classifier in the final step of the proposed approach. Table I gives the analytical definition of the six tree level IGFs derived from the internal branch structure model. Trees at various stages of their growth will have different branch lengths and hence we normalize the features such as B_l, B_k and B_w by the Tree Height H_T. The average branch density B_n is divided by N in order to filter out variations caused by point cloud density.

TABLE I: Proposed Internal Crown Geometric Features

Feature Id	Description	Equation
B_α	Average branch slope	$\frac{\sum_{b=1}^{B} \alpha_b}{B}$
B_l	Average branch length	$\frac{\sum_{b=1}^{B} L_b}{B \cdot H_T}$
B_k	Average branch compactness	$\frac{\sum_{b=1}^{B} K_b}{B \cdot H_T}$
B_w	Average branch width	$\frac{\sum_{b=1}^{B} W_b}{B \cdot H_T} = \frac{\sum_{b=1}^{B} \lambda_2^b}{B \cdot H_T}$
B_s	Average branch symmetry	$\frac{\sum_{b=1}^{B} S_b}{B} = \frac{\sum_{b=1}^{B} \frac{\lambda_2^b}{\lambda_3^b}}{B}$
B_n	Average branch density	$\frac{\sum_{b=1}^{B} D_b}{B \cdot N}$

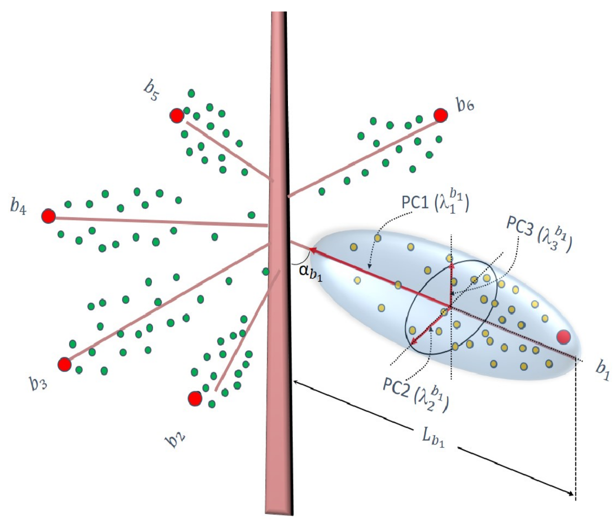

Fig. 5: Illustration of the proposed branch model and of the related parameters.

B. External Crown Structure Characterization

High density LiDAR data also provide detailed level knowledge about the external shape of tree crown (see Fig. 3a). Among the state-of-the-art algorithms for extracting information about the external crown geometry, shape fitting and convex hull based are the most popular. EGFs, which are derived using parameters of a regression-fitted geometric shape [46] and convex hull [47], obtained against the point cloud of a tree, are effective for tree species classification [15]. Fitting geometric shapes allows to have an idea of the general crown shape, whereas convex hull provides the smallest 3D surface that contains all the data points of a tree and thus provides information such as the crown volume, the surface area and the density. Conifer species have a similar typical conical crown shape that in some studies has been described with a generalized cone or paraboloid [48] [13]. For this study, we assume a simple cone shape and focus on features that are derived after shape-fitting. Whatsoever, considering the similar conical crown shape of conifers, it is expected that external crown geometrical features (EGFs) are less informative than IGFs, for species classification.

In order to fit a cone to the LiDAR point cloud of a tree, four cone parameters need to be estimated. These include the three coordinates of the cone vertex $V_c = [x_c, y_c, z_c]$, and the cone angle $a = tan(\alpha) = \frac{r}{h}$, where the angle α is the opening angle (semi-vertical angle),and r and h are the base radius and height of the cone (i.e. conifer in this case) respectively [49]. The general equation of a cone can be written as

$$(x_i - x_c)^2 + (y_i - y_c)^2 = (z_i - z_c)^2 a^2, \forall i \in [1, N] \quad (2)$$

where, x_i, y_i, z_i are Euclidean coordinates of the i^{th} LiDAR point sample in the tree. The parameters of the best fitting cone (see Fig. 6a) can be obtained by fulfilling the least square condition:

$$\hat{a} = \underset{a}{\operatorname{argmin}} \sum_{i=1}^{N} \epsilon_i^2 = \underset{a}{\operatorname{argmin}} \sum_{i=1}^{N} (a_i - a)^2 \quad \text{where,} \quad (3)$$
$$a_i = \sqrt{\frac{(x_i - x_c)^2 + (y_i - y_c)^2}{(z_i - z_c)^2}}$$

$\hat{a}$ is the optimal parameter value, obtained by fulfilling the least square condition, defining the best-fit cone that represents the external crown shape for the tree approximately. The initial vertex coordinates can be chosen to be the spatial coordinates of the highest LiDAR data point in the cloud. The optimal vertex can be different from the initial coordinate and is updated accordingly with a_i (see equation 3) . Among the several EGFs available in the literature, we selected the six least correlated EGFs mentioned in [15]. The features are derived from the parameters of best fitting cone and convex hull. For each tree LiDAR point cloud. They include the following parameters:

(a) Volume of convex hull V_{hull}, divided by the number of points within the tree crown N.
(b) Difference between the convex hull volume and the fitted cone volume V_{cone}, to the convex hull volume.
(c) Regression error $RMSE_{cone}$ associated with the cone fitting. It can be computed by solving the $\left(A^T A\right)^{-1} A^T Q$, where A is the matrix derived from the derivatives of the Taylor expansion (which is applied to linearize the non-linear equation of the cone) of a_i around the cone vertex, V_c. The equation of a can be derived from (2), and Q is $(a_1, a_2, a_3, ..., a_N)$. The regression error associated with the least square cone fitting is a species dependent

feature, as it does not consider only the general shape of the tree, but also the point density and distribution inside the canopy of the tree.

(d) Average of the distance of each point d_n, to the closest facet of the convex hull.

(e) Standard deviation of distances from each point to the closest facet of the convex hull.

(f) Ratio between the crown height H_C and tree height H_T.

Table II summarizes the considered external crown geometric features and provide their equations.

TABLE II: External Crown Geometric Features

Feature Id	Description	Equation
T_v	Volume of the convex hull by the number of points within the crown [50].	$\frac{V_{hull}}{N}$
T_d	Difference between the convex hull and fitted cone volumes compared to the convex hull volume [50].	$\frac{V_{hull}-V_{cone}}{V_{hull}}$
T_ϵ	Root mean squared error from regression fitting of cone [50].	$\frac{RMSE_{Cone}}{N}$
T_l	Average of distance d_n of each LiDAR point to the closest facet of convex hull [50]	$\frac{\sum_{n=1}^{N} d_n}{N}$
T_σ	Standard deviation of orthogonal distances from each point to the convex hull [50].	$\sqrt{\frac{\sum_{n=1}^{N}(p_n-T_l)^2}{H_T}}$
T_h	Crown height divide by Tree height [50]	$\frac{H_C}{H_T}$

C. Conifer species classification

In the last step, IGFs (Table I) and EGFs (Table II) are given as input to an automatic classifier that associates each tree with its species. Although any classifier could be employed, we use the Support Vector Machine (SVM) as it is very efficient and versatile [51] and has been successfully used in remote sensing applications. Three different SVM configurations has been used. Sparse C-SVM with linear kernel enhances the magnitude of feature weights (i.e., the weights of the relevant features are accentuated while the weights of the non relevant ones are attenuated) and thus is good to understand feature relative relevance. Both single and multi-kernel SVM architectures using both linear and non-linear kernels have been considered with the objective of achieving the highest classification accuracy and hence used for feature quality assessment in this paper.The rest of the section briefly summarizes the theory of the above mentioned classifiers.

Let $\{\vec{\mathrm{v}}_{\mathrm{i}}\}_{i=1}^{N_G}$ be the set of training feature vectors. N_G is the total number of training samples and $\vec{\mathrm{v}}_{\mathrm{i}} \in R^d$, d is the number of features. Let $\{u_i\}_{i=1}^{N_G}$ be the set of corresponding class labels in the training set, where $u_i \in$ {-1 1}. In our case, the input vector $\vec{v_i}$ is defined as the normalized set of IGFs and EGFs, i.e., $\vec{v_i} = [B_\alpha, B_l, B_k, B_w, B_s, B_n, T_v, T_d, T_\epsilon, T_l, T_\sigma, T_h]$.

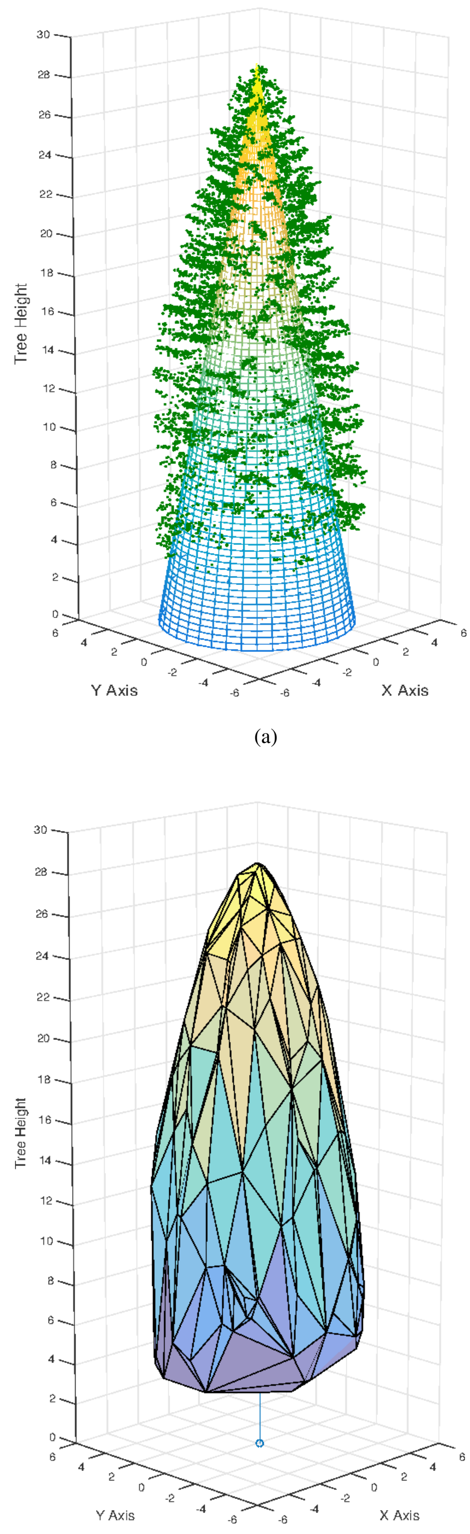

(a)

(b)

Fig. 6: Representation of (a) the regression cone fitting on the LiDAR point cloud of a Norway Spruce tree, and (b) shows the convex hull obtained for the same tree

.

The SVM aims at estimating an optimal separating hyperplane defined by the parameters $\vec{w}$ and e, which are the normal vector and the bias, respectively [43]. The estimates of $\vec{w}$ and e, for the C-SVM and MK C-SVM are obtained by solving the optimization problem in (4).

$$\begin{aligned} \min_{\vec{w},\xi,e} \quad & \frac{1}{2}t + C\sum_{i=1}^{N}\xi_i, \\ \text{subject to} \quad & u_i(\vec{w}^T f(v_i) + e) \geq 1 - \xi_i, \forall i = 1, \dots, N_G, \\ & \xi_i \geq 0, \end{aligned} \tag{4}$$

The function $f(v)$ for the C-SVM is a single kernel $K(v, v')$, whereas for the MK C-SVM it is a multiple kernel $\sum_{m=1}^{M} d_m K(v, v')$, where M is the number of kernels, and $\sum_{m=1}^{M} d_m = 1$. K(.,.) is a given positive definite kernel associated with a reproducing kernel Hilbert space. In our case we use Radial Basis Function (RBF) kernel for both C-SVM and MK C-SVM. The terms ξ and C in (4) are the slack variables and the tuning parameter, respectively. Linear Sparse C-SVM performs classification by exploiting the sparsity in the input feature space, and emphasises the relevance of features (i.e., their weights), while reducing the relevance of noisy and/or correlated features. In the case of Sparse C-SVM, the optimal feature selection and the SVM learning processes are achieved simultaneously. Although popular in other fields, Sparse C-SVM has not been widely used in remote sensing and hence we provide some details on it. The estimates of $\vec{w}$ and e are obtained by solving the optimization problem in (5).

$$\begin{aligned} \min_{\vec{w},\xi,e,t} \quad & \frac{1}{2}t + C\sum_{i=1}^{N}\xi_i, \\ \text{subject to} \quad & u_i(\vec{w}^T f(v_i) + e) \geq 1 - \xi_i, \forall i = 1, \dots, N_G, \\ & \xi_i \geq 0, \\ & ||\vec{w}||_2^2 \leq t \\ & ||\vec{w}||_1^2 \leq rt \end{aligned} \tag{5}$$

The Sparse C-SVM formulation shown in (5) is the same as that of the C-SVM or MK C-SVM (4) except for the two additional constraints on $\vec{w}$. The (5) is rather a simplified version of the original optimization problem in [42]. The simplification of the problem is achieved by replacing the cardinality constraint in the original problem with a weaker non-convex constraint, i.e., $||\vec{w}||_1^2 \leq \sqrt{r}||\vec{w}||_2^2$ [42]. This weaker non-convex constraint can be further relaxed to a convex form by bounding the norm $L2$ constraint on $\vec{w}$ by a variable t, and the $L1$ norm constraint on $\vec{w}$ by rt, where t is a constant. Hence, the aforementioned non-convex constraint can be split into the following constraints $||\vec{w}||_2^2 \leq t$ and $||\vec{w}||_1^2 \leq rt$ [42]. The $L1$ constraint on weight vector $\vec{w}$ allows it to be Sparse (i.e., some values of $\vec{w}$ could be 0), while the $L2$ constraint minimizes the number of elements of $\vec{w}$ to be shrunk to zeros. Hence, only few relevant features are considered while generating the hyperplane. The individual elements of $\vec{w}$ quantify the relative importance of a feature with respect to the others.

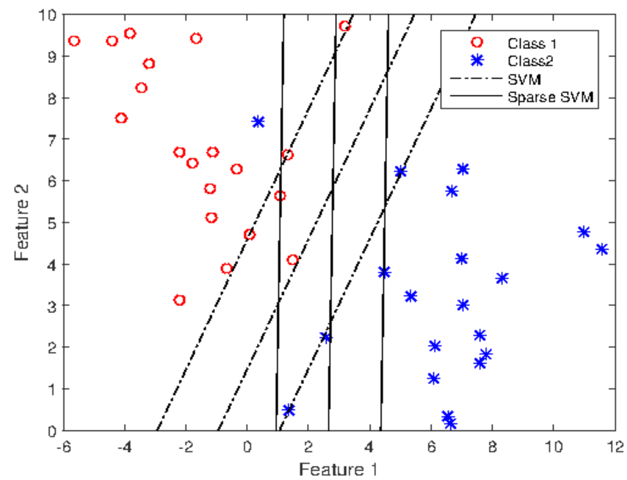

Fig. 7: Illustration of the hyperplanes formed by the C-SVM and the Sparse C-SVM in an R^2 space. The Sparse C-SVM ignores one dimension (i.e. Feature 2).

Fig. 7 shows an illustration of the hyperplanes obtained with a standard linear SVM and a linear Sparse C-SVM for a 2-class 2D problem. C-SVM considers both the features 1 and 2 to define the hyperplane, whereas linear Sparse C-SVM creates the hyperplane based on the feature 1 only. Similar considerations hold for a higher dimensional feature space. Using a subset of the original features makes the process computationally more efficient, at the cost of a small decrease in the classification accuracy w.r.t. C-SVM or MK C-SVM. If a multi-class problem needs to be solved, one-against-one or one-against-all approaches can be employed as for standard linear SVM [52].

IV. Experimental Results and Discussion

A. Study Area and Data Set

The study area is located in the Italian Alps, in the municipality of Pellizzano at about 40 km northwest of Trento (a city in the North of Italy). The area contains valleys and mountainous terrains. The approximate extent of the area is about 3200 ha, and the altitude varies from 900 to 2000 m above the sea level. The forest in this region is heterogeneous with both coniferous and broad-leaf species. The dominant coniferous species include the Norway Spruce (Picea abies), the European Larch (Larix decidua), the Swiss Pine (Pinus cembra) and the Silver Fir (Abies alba). Minority coniferous species are European Black Pine (Pinus nigra) and Scots Pine (Pinus sylvestris). Among the broadleaf species European Beech (Fagus sylvatica L.) dominates over Sycamore Maple (Acer pseudoplatanus L.), Hop Hornbeam (Ostrya carpinifolia Scop.), Field Elm (Ulmus campestris), and Sessile Oak (Quercus petraea Liebl). Here attention is devoted only to the four major coniferous species. The LiDAR data were acquired between 7^{th} and 9^{th} September 2012 from an airborne platform flying at an altitude of 660 m with a speed of 100 Km/Hr. The acquisition sensor is a Riegl LMSQ680i. The frequency of the laser scanner is 400 KHz and up to four returns were recorded. The point density varies from 10-50 points per meter squared due to the mountainous terrain of the study area. The flight was repeated several times to generate a dense point cloud with density varying from 50 to 200 points/m^2. As expected, a high density point cloud is observed below the flight path (i.e., near nadir) whereas the density of the point cloud decreases off-nadir. The density of LiDAR points is maximum in the crown region and reduces toward the interior section of the trees. Further, point density is maximum near the tree top and minimum at the bottom. The ground sample collection was conducted in the same month as that of the data acquisition. Among them, a set of 200 reference trees, manually delineated from the point cloud, was created, that includes 50 trees each of the Norway Spruce (NS), the European Larch (EL), the Swiss Pine (SP) and the Silver Fir (SF) species. On the one hand, the NS, EL, and SF are relatively tall trees and are geometrically more similar to the assumed conifer characteristics. On the other hand, the SP is shorter with slightly different characteristics. SP class is included in the study as: a) it is one of the major species in Europe, and 2) it allows to evaluate the robustness of the proposed modelling technique. Table III shows the tree and crown height statistics of the tree samples. In order to validate the effectiveness of the proposed internal crown model and of the features derived from it, the crown of trees in the reference set was manually detected. In this way, the validation procedure does not suffer from: 1) propagation of error due to automatic tree delineation techniques and, 2) the presence of structurally damaged trees (as this is not investigated in this research). However, for operational use, automatic segmentation methods [5], [25], [27] can be employed, followed by a noise filtering to avoid isolated points around the crown. LiDAR points corresponding to understory vegetation were manually removed (but automatic methods from the literature can be employed as well [53], [27]) since they do not follow the conifer crown model. Selected trees show in average 12000 points from multiple scanning passes.

TABLE III: Basic statistics of the structural characteristics of the sample conifer on the considered dataset

Tree Species	Number of Trees	Tree height (m)			Crown height (m)		
		Max	Min	Mean	Max	Min	Mean
NS	50	44.97	22.36	31.51	35.0	19.0	26.31
EL	50	37.64	16.92	28.32	30.0	15.0	21.84
SP	50	39.57	13.49	30.35	34.0	10.0	24.52
SF	50	23.66	10.51	17.56	20.0	9.56	15.53

B. Experimental Results and Discussion

A direct evaluation of the performance of the proposed internal crown modelling technique would require reference information at the branch level. However this is not feasible as it would require a very accurate branch level field data collection. Thus, we adopted a validation set that includes qualitative analysis and an indirect quantitative assessment. The results obtained using the proposed internal crown model are compared with the ones obtained by relying on a state-of-the-art (SoA) one. Merge and Split K-means clustering approach to internal crown structure modelling is used as the SoA method [15]. It applies k-means clustering to LiDAR data with random seed initialization, and performs a merging and splitting operations on the cluster to identify final valid branch clusters. In our experiments, the k has been set to be equal to the number of branch-tips identified using the proposed technique. For each tree, the branch tips were identified using the convex hull based technique with the variance parameter set to 0.5. The threshold (at crown bottom height) for multiple branch tip removal was set to 2.0, 3.8, 2.8 and 1.9 for NS, EL, SP and SF, respectively. In this way, we give clear advantage to the reference technique that has not the intrinsic capability to estimate the number of expected branches. The reader is referred to [15] for further details on the merge and split k-means based branch detection approach. In our method, the branch clusters were identified using the region growing performed on the point cloud, starting from the identified seed points. The growing is stopped when the neighbourhood threshold density becomes lower than the 0.3% of the density near the branch tip (where the density is likely to be the maximum). K was set to 5 for all the cases.

From the qualitative point of view, a visual comparison of the internal crown model obtained with the proposed model and with the SoA one was conducted for several trees in the reference set. Figures 8, 9, 11, 10 show examples of: a) the tree LiDAR point cloud, b) the branch model obtained with the SoA approach, and c) the branch model obtained with the proposed approach, for each of the four considered species. It can be observed that the proposed model is able to better capture the branch structure for all the considered species. This becomes more clear in the upper right part of Fig. 8. It can be observed that all the branch clusters have been correctly captured by the proposed method, whereas the SoA method fails to do so. The poor modelling capability of the SoA model is mainly caused due to isotropic groping preferences and random initialization of the k-means clustering. This choice, combined with the complexity of the LiDAR point cloud, often make it difficult to identify valid branch clusters. The proposed model overcomes the drawbacks by employing the convex hull based technique. Recalling that IGFs are attributes associated to the branches, their reliability depends on the branch model accuracy. Accordingly, it is expected that IGFs extracted from the SoA branch model are less reliable than the ones extracted from the proposed one while classifying species.

In order to quantitatively assess the above statement, IGFs were extracted by employing both the proposed and the SoA internal crown model. The EGFs were computed as well. An indirect quantitative validation of both the internal crown structural model and the proposed IGFs was achieved by analyzing: i) the feature weights estimated during the Sparse C-SVM training phase; and ii) the Sparse C-SVM, C-SVM and MK C-SVM classification accuracy. The experiments were conducted on the following feature combinations: i) External Crown Geometric Features (EGFs); ii) IGFs extracted from the state-of-the-art model (IGFs-SoA); iii) IGFs extracted from the proposed internal crown model (IGFs-proposed); iv) IGFs

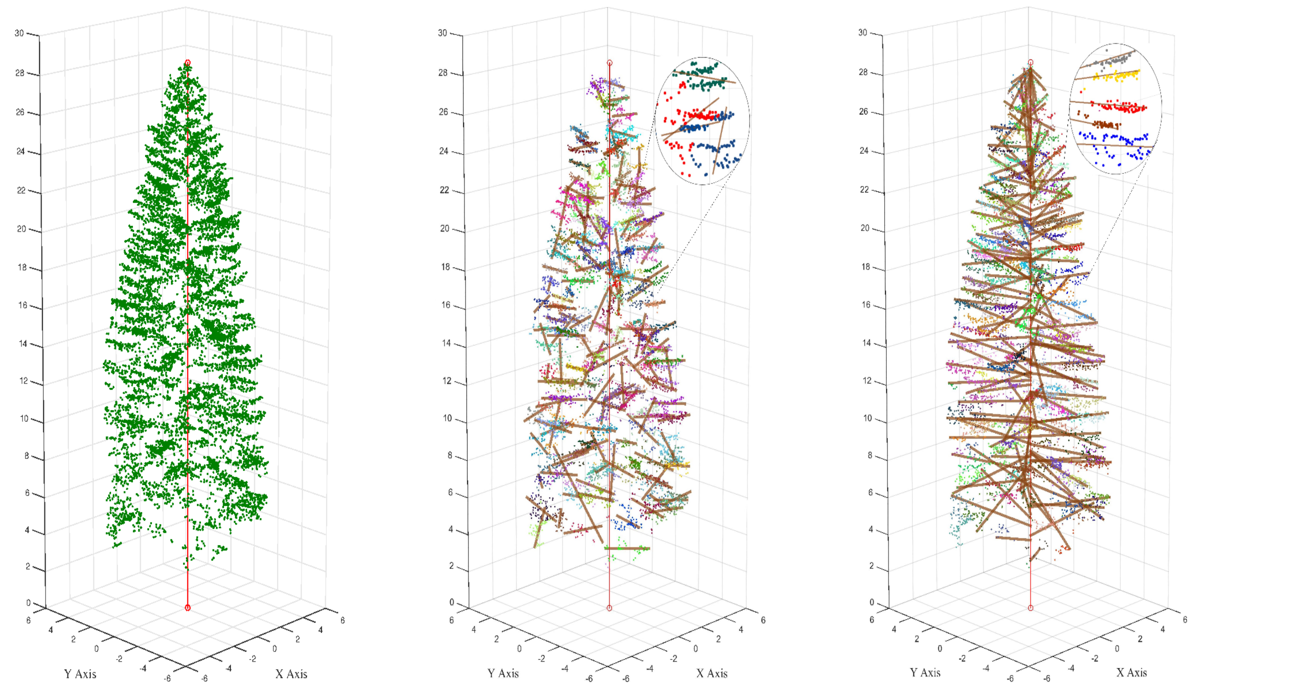

(a) (b) (c)

Fig. 8: Example of results on a Norway spruce tree, (a) show the raw LiDAR data, (b) the results obtained by the SoA model, (c) the results obtained by the proposed model.

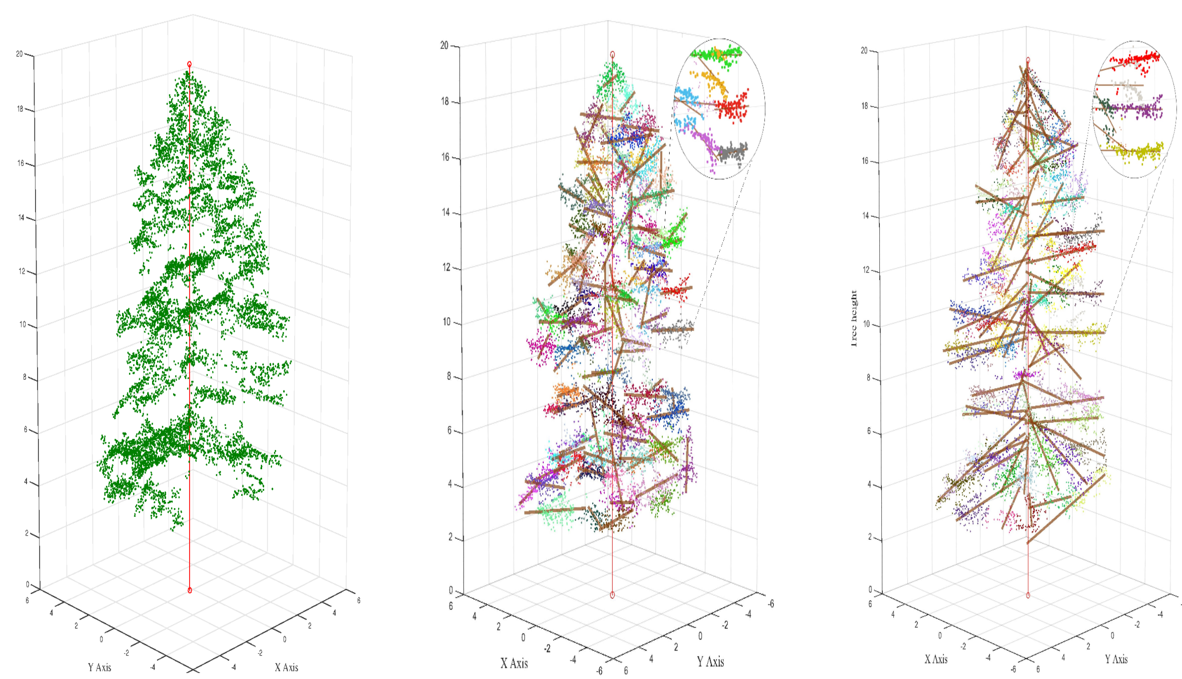

(a) (b) (c)

Fig. 9: Example of results on a European larch tree, (a) show the raw LiDAR data, (b) the results obtained by the SoA model, (c) the results obtained by the proposed model.

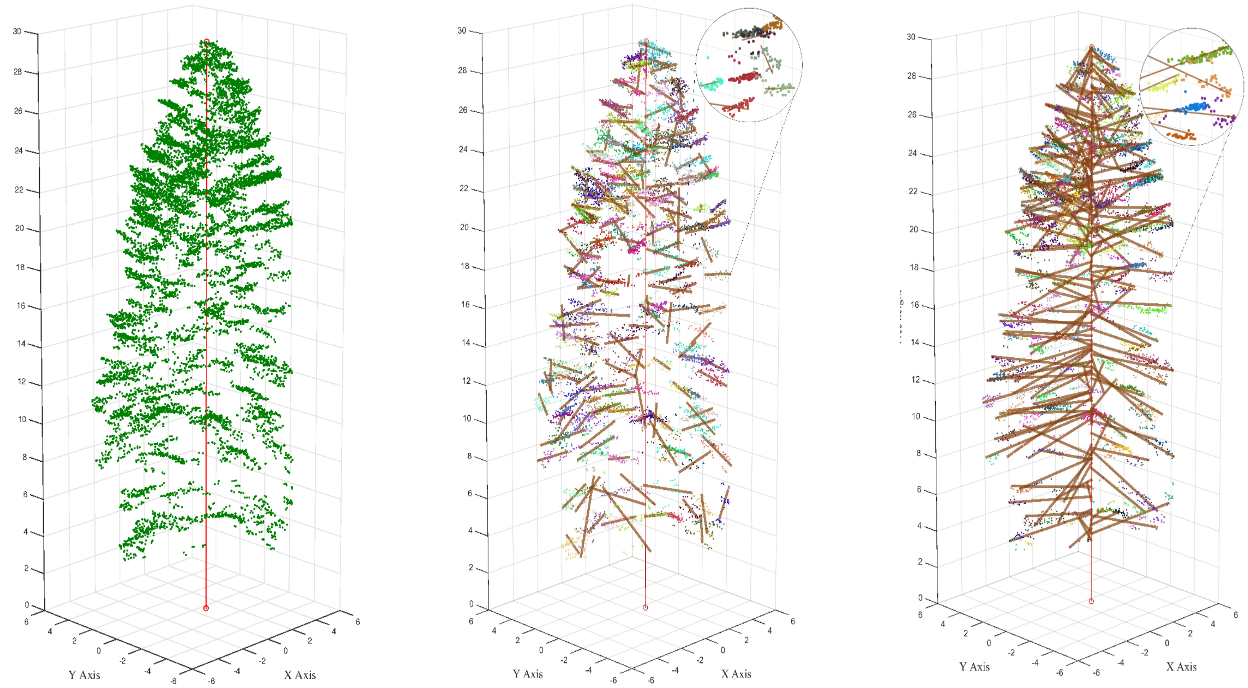

(a) (b) (c)

Fig. 10: Example of results on a Swiss pine tree, (a) show the raw LiDAR data, (b) the results obtained by the SoA model, (c) the results obtained by the proposed model.

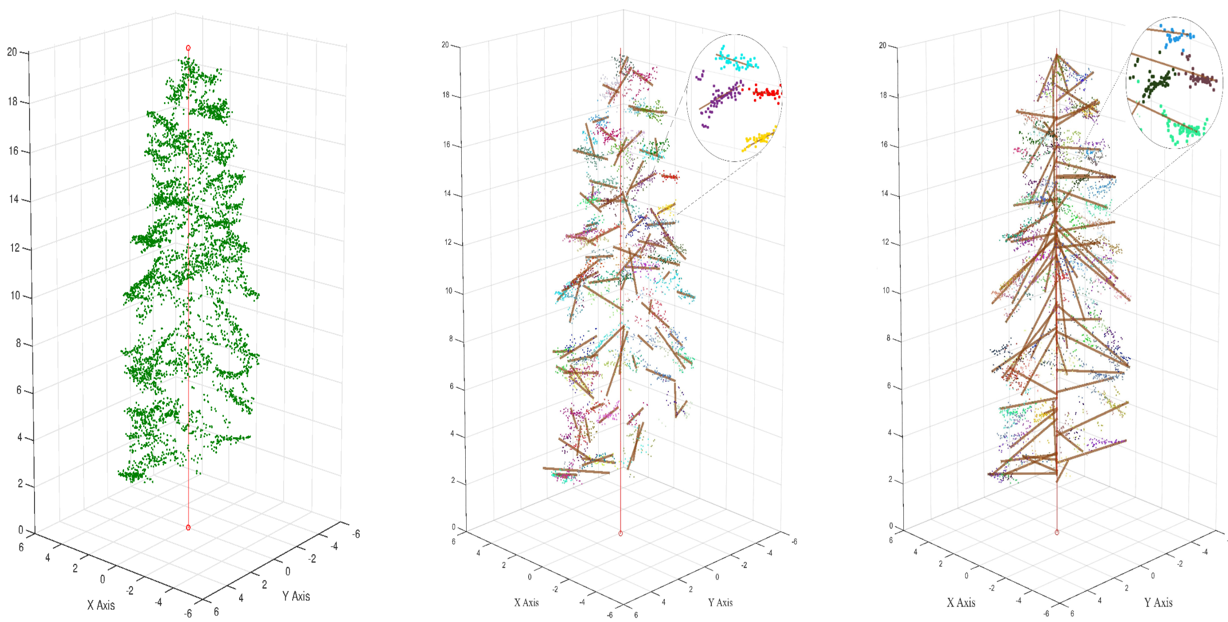

(a) (b) (c)

Fig. 11: Example of results on a Silver fir tree, (a) show the raw LiDAR data, (b) the results obtained by the SoA model, (c) the results obtained by the proposed model.

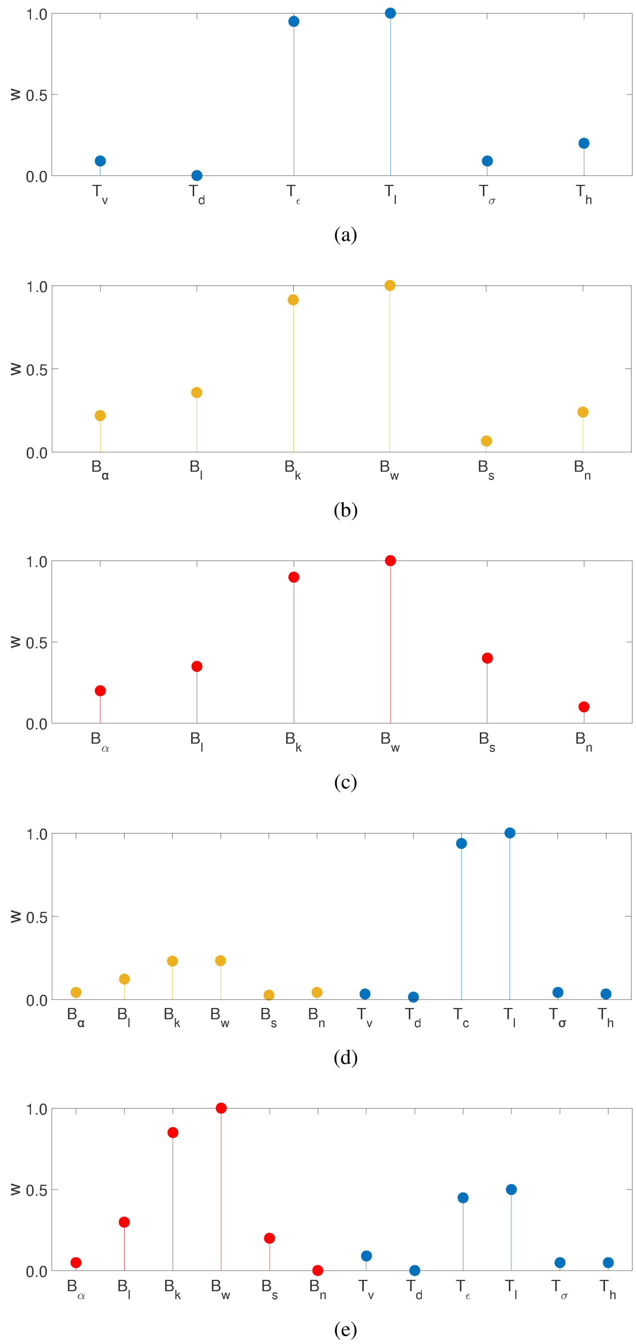

Fig. 12: The Sparse C-SVM weights obtained when employing: (a) only EGFs, (b) only IGFs computed on the SoA model (c) only IGFs computed on the proposed model, (d) the IGFs from the SoA model together with the EGFs, and (e) the IGFs from the proposed model together with the EGFs.

extracted from the state-of-the-art model and the EGFs (IGFs-SoA and EGFs); and v) IGFs extracted by the proposed internal crown model and the EGFs (IGFs-proposed and EGFs). For all the cases the better the performance, the better is the considered set of features and thus the corresponding internal crown model. The feature extraction step requires about 15 seconds for each tree on a 64-bit Windows 10 machine with 8.00 GB of RAM and Intel Xeon CPU E3-1240 V2. Thus, for operational use, the performance can be improved using parallel computing.

For all the classifiers, the training was conducted by means of a 4-fold cross-validation. The 60% of the total samples (i.e., 120 trees) were employed in the cross-validation procedure, and the remaining 40% (i.e., 80 trees) was used for validation. The validation set was selected such that 20 trees for each of the four species were included. Considering that the sample dataset size is small, the process was repeated 20 times and the results are analysed as the average over the 20 runs. The training procedure aimed at estimating: i) the optimal C parameter for each classifier, and ii) the optimal kernel parameters for C-SVM and MK C-SVM. Here an RBF kernel was used, thus the spread γ of the kernel(s) was estimated. For Sparse C-SVM, C values were considered in the range [10^{-6}, 10^{6}] with an exponential step of 10^1. For all combination of features, the best average accuracy on the validation set was found for $C = 10^5$. For C-SVM, C was considered in the range [2^{-15}, 2^{15}] with an exponential step of 2^1, whereas γ varied in the range [0.001, 10] with an exponential step of 10^1. The best average accuracy was achieved with $C = 2^8$ and $\gamma = 0.01$ for the EGFs, the IGF-SOA and the IGF-Proposed feature sets, and with $C = 2^9$ and $\gamma = 0.01$ for the remaining sets. For MK C-SVM, C was considered in the range [2^{-15}, 2^{15}] with an exponential step of 2^1 (like for the C-SVM), and a total of 9 RBF kernels were selected. The 9 corresponding γ values were selected by using the C-SVM optimal γ value as a guideline. Accordingly, γ values for MK C-SVM were selected close to 0.01 (i.e., 0.002, 0.004, 0.006 ,0.008, 0.010, 0.012, 0.014, 0.016 and 0.018). It is worth noting that the input data are from a single source and hence large variations in γ are not expected. The optimal C for MK C-SVM was found to be 2^{10}. Feature values were normalized before giving them as input to the classifiers [56].

Let us first analyse the feature relevance obtained as the weights of the trained Sparse C-SVM (linear soft margin, implemented using CVX [55]). The feature weights are a result of the class separability analysis performed by the Sparse C-SVM, i.e., a higher feature weight shows that the feature is relatively more relevant when compared to the others [54]. The weight values for most EGFs are small and thus they are less relevant for conifer species classification (see Fig. 12a). This behavior was expected as conifers have very similar external crown characteristics. Nonetheless, the cone fit error (T_ϵ) and the average distance of LiDAR points to the closest facade of the convex hull (T_l) showed to be promising features and this agrees with our observation that the crown shape and the point density variation around the stem are slightly different for different species. Fig. 12c shows the normalized features weights obtained in the proposed set up. The Sparse C-SVM assigned maximum weights to the branch width B_w and average branch compactness B_k. This is in alignment with our visual examination (a close look at Fig. 8, 9, 11, 10 shows that each tree species shows a unique branch width and branch compactness). Both B_w and B_k are independent of variations in both the point cloud density and the maturity of the tree, and hence are good features for species classification. While the average branch slope B_α, the average branch length B_l, the average branch symmetry B_s, and the average branch density B_n, were assigned lower weights. This implies that the B_l and B_α are less useful features at least for discriminating the species considered in this study. In case of B_α, the low weight value is a result of variation in branch slopes along its height. The low weight values for B_l is connected to the fact that trees of the same species and similar height can vary in their crown diameter, and thus show different branch lengths. Although, the average branch symmetry was expected to be a good feature to classify tree species, the results proved that they are less relevant for the four species considered in this study. This is attributed to the fact that branches of different species have similar ratio values. For example, the Norway spruce and the Silver Fir seem to have different branch sizes. However the ratio between the branch width and the branch height is very similar. The average branch density is a good feature for species classification if the LiDAR sampling density is uniform throughout the acquisition, However in our case, the large variation in the point cloud density makes it less relevant with the current set of species.

It is worth noting at this point that the weight values show only the relative importance of the features, and hence a direct comparison of the values across experiments involving different set of features is meaningless. However by jointly providing as input the IGFs-proposed and the EGFs to the Sparse C-SVM, it is possible to compare the importance of the IGFs-proposed and the EGFs. The Fig. 12e shows the weight obtained for this feature combination. It is evident that the EGFs have been identified as relatively less important than the IGFs-proposed.

The normalized weight values obtained for the IGFs-SoA are shown in Fig. 12b. The features B_k and B_w have higher values and hence are more relevant. This is in line with our expectation for the same reasons mentioned previously. B_l, B_α, B_s and B_n have relatively smaller weights. We also tested the case in which the IGFs-SoA along with the EGFs were provided as input to the Sparse C-SVM. The Fig. 12d shows the normalized feature weights. As one can see, the EGFs were assigned higher weight values than any of the features in the IGFs-SoA set. The box-plots in Fig. 13 confirm the quantitative separability analysis. It can be seen that the highest weights are assigned to those features with non-overlapping means and minimum variance.

Since EGFs are extracted independently of branch geometric model, they can act as a benchmark for feature quality comparison between the IGFs-SoA and the IGFs-proposed features. By comparing weight assignments for the IGFs-SoA and the EGFs, and IGF-proposed and the EGFs, one can see that the IGFs-SoA have been identified as poor features in comparison to the EGFs whereas the IGFs-proposed proved to be better features than the same EGFs.

Let us now compare the average classification accuracy computed over the 20 runs and obtained on the five feature sets by using the Sparse C-SVM, the C-SVM (LIBSVM [57]) and the MK C-SVM (SimpleMKL Matlab tool [58]). Table IV summarizes quantitative results. It is clear from Table IV that the classification performance is higher when using the IGFs-proposed set rather than the IGFs-SoA feature set, both with and without the EGFs. This means that the proposed model is more accurate than the SoA one. Therefore the features derived from the proposed internal crown model are more effective.

TABLE IV: Average classification accuracy on the validation set for different sets of features.

Feature Set	**Classification Accuracy (%)**		
	Sparse C-SVM	**C-SVM**	**MK C-SVM**
EGFs	68.5	72.2	71.5
IGFs-SoA	75.8	79.2	79.7
IGF-proposed	81.2	86.0	86.6
IGFs-SoA and EGFs	80.9	86.9	87.7
IGF-proposed and EGFs	85.3	89.1	89.5

Furthermore, IV points out that the MK C-SVM performs better w.r.t the Sparse C-SVM and C-SVM. Thus, we evaluate the species classification performance based on the accuracy provided by the MK C-SVM. As expected, the use of the EGFs only led to lower performance, i.e., an overall accuracy of 71.5%. An increment of performance of about 8.0% and 15.0% was achieved when using the IGFs-SoA and the IGFs-proposed feature sets, respectively. It is worth noting that the use of the proposed internal structural model significantly increased the overall classification accuracy, with respect to the use of features derived from the state-of-the-art one. This improvement confirms the effectiveness of both of the proposed internal structural model and the proposed IGFs. When both the IGFs and the EGFs are given as input to the Sparse C-SVM, the classification accuracy increases further reaching 87.7% with the IGFs-SoA features, and 89.5% with the IGFs-proposed features. The accuracy improvement achieved by the joint use of EGFs and IGFs is of about 8.0% and 3.0% when the state-of-the-art and the proposed model are used, respectively. Tables V and VI show the confusion matrices (including user's accuracy (U.A.) and producer's accuracy (P.A.)) for the IGFs-SoA and the EGFs, and the IGFs-proposed and the EGFs experiments, respectively. The best result over the 20 runs was selected. As one can see, the number of errors is smaller for all the species when using the IGFs-proposed feature set.

TABLE V: MK C-SVM confusion matrix of the best case over 20 runs on using the IGFs-SoA and the EGFs feature set.

Classification	Field Data				U.A.%
	NS	EL	SP	SF	
NS	17	0	2	1	85.0
EL	0	19	1	0	95.0
SP	1	0	19	0	95.0
SF	2	0	1	17	85.0
P.A.%	85.0	100.0	100.0	82.6	O.A. 90.0 %

V. Conclusion

In this paper, we proposed a method for modelling the internal crown structure of the conifers from small footprint high point density multi-return airborne LiDAR point clouds. The internal crown structure modelling is performed using a set of six novel features capable of characterizing the individual

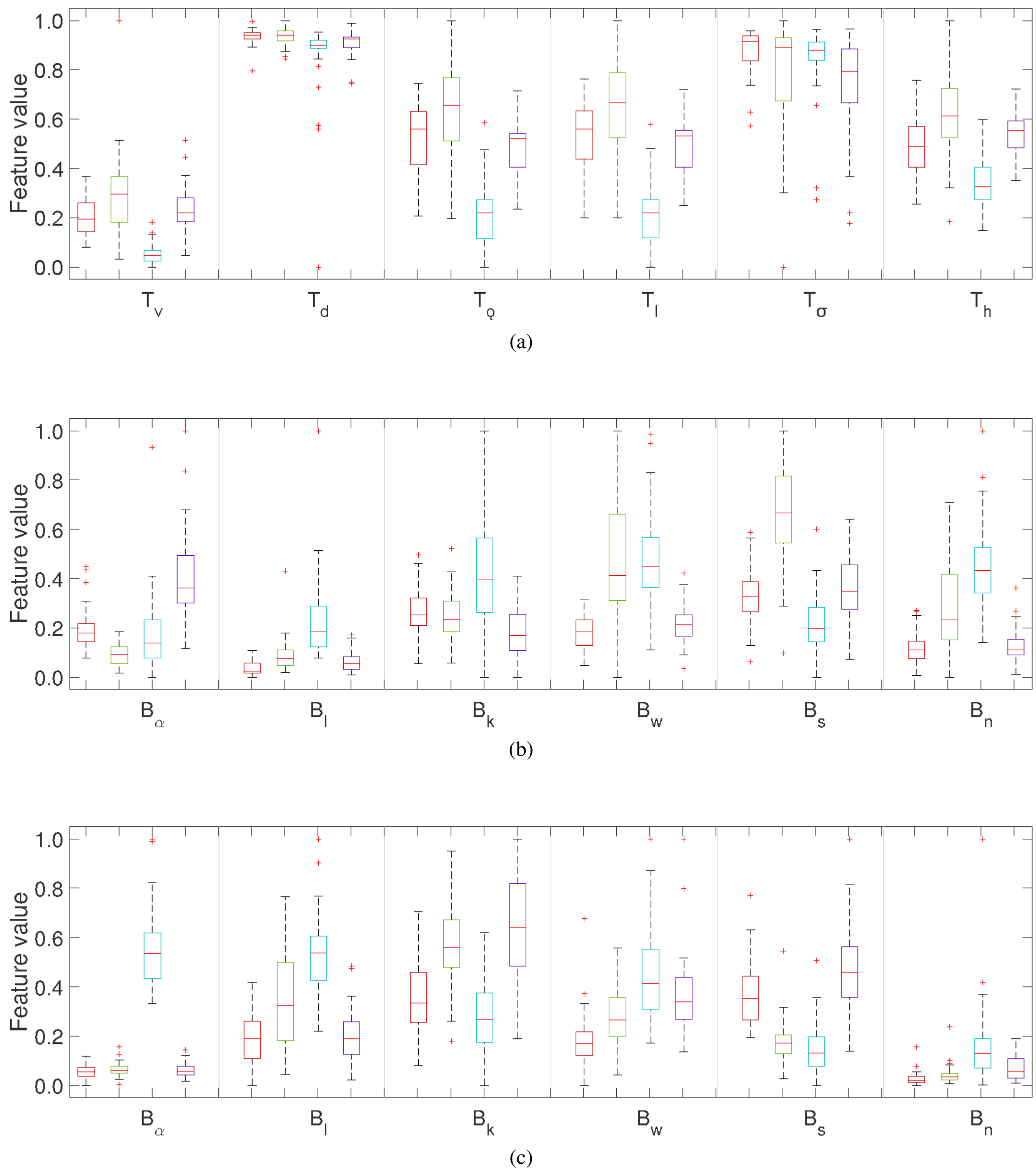

Fig. 13: Box plot analysis of (a) EGFs, (b) IGFs-SoA and (c) IGFs-proposed, for Norway spruce (red color), European larch (green color), Swiss pine (light blue color) and Silver fir (purple color), respectively.

TABLE VI: MK C-SVM confusion matrix of the best case over 20 runs on using the IGFs-proposed and the EGFs feature set.

Classification	Field Data				U.A.%
	NS	EL	SP	SF	
NS	18	1	0	1	90.0
EL	0	19	0	1	95.0
SP	0	0	20	0	100.0
SF	2	0	0	18	90.0
P.A.%	90.0	95.0	100.0	90.0	O.A. 93.7 %

branch. The six proposed features are jointly used with six external crown geometric features taken from the literature for improving the classification accuracy by modelling also the external crown geometry of the trees. Accuracy assessment was performed by using three different SVM classifier including the Sparse C-SVM, the C-SVM, and the MK C-SVM. A set of five experiments were conducted to study the individual and the joint performance achieved by using the proposed and standard features taken from the literature. All experiments were conducted on a set of 200 tree samples belonging to the four major European conifer species (i.e., the Norway Spruce, the European Larch, the Swiss Pine, and the Silver Fir). Experimental results point out that the proposed internal crown model leads to the generation of more effective features with respect to the state-of-the-art one. Furthermore, the joint use of the proposed internal crown geometric features together with standard external crown geometric features provides sharply higher classification accuracies in conifer species classification than the use of external crown geometric features only. This proves the effectiveness of the proposed method that makes it possible to obtain satisfactory results in species classification without the use of any multispectral or hyperspectral image. As future works, we plan to design additional internal crown geometric features to improve conifer species classification accuracy and to consider the effects of crown-overlap and under-story vegetation on the modelling process and hence on the final classification accuracy. Moreover, we plan to extend the method to characterize partially damaged trees (e.g., trees with missing branches and/or having unsymmetrical crown shapes).

References

[1] S. E. Taylor, T. P. McDonald, M. W. Veal, and T. E. Grift, "Using gps to evaluate productivity and performance of forest machine systems," in *Presented at the first international precision forestry symposium*, Seattle, WA, USA, Jun. 17–19, 2001.

[2] K. Anitha, S. Joseph, R. J. Chandran, E. Ramasamy, and S. N. Prasad, "Tree species diversity and community composition in a human-dominated tropical forest of western ghats biodiversity hotspot, india," *Ecol. Complexity*, vol. 7, no. 2, pp. 217–224, Feb. 2010.

[3] A. Gebrekirstos, R. Mitlöhner, D. Teketay, and M. Worbes, "Climate–growth relationships of the dominant tree species from semi-arid savanna woodland in ethiopia," *Trees*, vol. 22, no. 5, pp. 631–641, Apr. 2008.

[4] G. Sohn and I. Ituen, "The way forward: Advances in maintaining right-of-way of transmission lines," *Geomatica*, vol. 64, no. 40, pp. 451–462, Dec. 2010.

[5] J. Hyyppä, O. Kelle, M. Lehikoinen, and M. Inkinen, "A segmentation-based method to retrieve stem volume estimates from 3-d tree height models produced by laser scanners," *IEEE Trans. Geosci. Remote Sens.*, vol. 39, no. 5, pp. 969–975, May. 2001.

[6] M. J. Falkowski, J. S. Evans, S. Martinuzzi, P. E. Gessler, and A. T. Hudak, "Characterizing forest succession with lidar data: An evaluation for the inland northwest, usa," *Remote Sens. Environ.*, vol. 113, no. 5, pp. 946–956, May. 2009.

[7] M. Dalponte, H. O. Ørka, L. T. Ene, T. Gobakken, and E. Næsset, "Tree crown delineation and tree species classification in boreal forests using hyperspectral and als data," *Remote sensing of environment*, vol. 140, pp. 306–317, 2014.

[8] T. Brandtberg, "Classifying individual tree species under leaf-off and leaf-on conditions using airborne lidar," *ISPRS J. Photogramm. Remote Sens.*, vol. 61, no. 5, pp. 325–340, Jan. 2007.

[9] S. Kim, T. Hinckley, and D. Briggs, "Classifying individual tree genera using stepwise cluster analysis based on height and intensity metrics derived from airborne laser scanner data," *Remote Sens. Environ.*, vol. 115, no. 12, pp. 3329–3342, Dec. 2011.

[10] Y. Lin and J. Hyyppä, "A comprehensive but efficient framework of proposing and validating feature parameters from airborne lidar data for tree species classification," *International Journal of Applied Earth Observation and Geoinformation*, vol. 46, pp. 45–55, Apr. 2016.

[11] M. Dalponte, L. Bruzzone, and D. Gianelle, "Tree species classification in the southern alps based on the fusion of very high geometrical resolution multispectral/hyperspectral images and lidar data," *Remote Sens. Environ.*, vol. 123, pp. 258–270, Aug. 2012.

[12] J. Holmgren, Å. Persson, and U. Söderman, "Species identification of individual trees by combining high resolution lidar data with multi-spectral images," *Int. J. Remote Sens.*, vol. 29, no. 5, pp. 1537–1552, Mar. 2008.

[13] C. Paris and L. Bruzzone, "A three-dimensional model-based approach to the estimation of the tree top height by fusing low-density lidar data and very high resolution optical images," *IEEE Trans. Geosci. Remote Sens.*, vol. 53, no. 1, pp. 467–480, Jan. 2015.

[14] P. Hyde, R. Dubayah, W. Walker, J. B. Blair, M. Hofton, and C. Hunsaker, "Mapping forest structure for wildlife habitat analysis using multi-sensor (lidar, sar/insar, etm+, quickbird) synergy," *Remote Sens. Environ.*, vol. 102, no. 1, pp. 63–73, May. 2006.

[15] C. Ko, G. Sohn, and T. K. Remmel, "Tree genera classification with geometric features from high-density airborne lidar," *Can. J. Remote Sens.*, vol. 39, no. sup1, pp. S73–S85, Jun. 2013.

[16] E. Naesset, "Determination of mean tree height of forest stands using airborne laser scanner data," *ISPRS J. Photogramm. Remote Sens.*, vol. 52, no. 2, pp. 49–56, Apr. 1997.

[17] Z. Rahman, M and B. Gorte, "Individual tree detection based on densities of high points of high resolution airborne lidar," in *Proceedings GEOBIA, 2008 - Pixels, Objects, Intelligence: GEOgraphic Object Based Image Analysis for the 21st Century*. University of Calgary, Calgary, Alberta, Canada, 5-8 Aug. 2008, pp. 350–355.

[18] C. E. Woodcock, J. B. Collins, S. Gopal, V. D. Jakabhazy, X. Li, S. Macomber, S. Ryherd, V. J. Harward, J. Levitan, Y. Wu *et al.*, "Mapping forest vegetation using landsat tm imagery and a canopy reflectance model," *Remote Sens. Environ.*, vol. 50, no. 3, pp. 240–254, Dec. 1994.

[19] D. S. Culvenor, "Tida: an algorithm for the delineation of tree crowns in high spatial resolution remotely sensed imagery," *Comput. Geosci.*, vol. 28, no. 1, pp. 33–44, Feb. 2002.

[20] M. Wulder, K. O. Niemann, and D. G. Goodenough, "Local maximum filtering for the extraction of tree locations and basal area from high spatial resolution imagery," *Remote Sens. Environ.*, vol. 73, no. 1, pp. 103–114, Jul. 2000.

[21] L. Wang, W. P. Sousa, P. Gong, and G. S. Biging, "Comparison of ikonos and quickbird images for mapping mangrove species on the caribbean coast of panama," *Remote Sens. Environ.*, vol. 91, no. 3, pp. 432–440, Jun. 2004.

[22] S. Solberg, E. Naesset, and O. M. Bollandsas, "Single tree segmentation using airborne laser scanner data in a structurally heterogeneous spruce forest," *Photogrammetric Engineering & Remote Sensing*, vol. 72, no. 12, pp. 1369–1378, Dec. 2006.

[23] J. Reitberger, M. Heurich, P. Krzystek, and U. Stilla, "Single tree detection in forest areas with high-density lidar data," *International Archives of Photogrammetry, Remote Sensing and Spatial Information Sciences*, vol. 36, no. 3, pp. 139–144, Sep. 2007.

[24] Z. Rahman, M, B. Gorte, and A. Bucksch, "A new method for individual tree delineation and undergrowth removal from high resolution airborne lidar," *in Proc. IARPS*, vol. 38, no. 3, pp. 283–288, Sep. 2009.

[25] U. Pyysalo and H. Hyyppa, "Reconstructing tree crowns from laser scanner data for feature extraction," *International Archives Of Photogrammetry Remote Sensing And Spatial Information Sciences*, vol. 34, no. 3/B, pp. 218–221, Sep. 2002.

[26] M. J. Falkowski, A. M. Smith, A. T. Hudak, P. E. Gessler, L. A. Vierling, and N. L. Crookston, "Automated estimation of individual conifer tree height and crown diameter via two-dimensional spatial wavelet analysis of lidar data," *Can. J. Remote Sens.*, vol. 32, no. 2, pp. 153–161, Jan. 2006.

[27] V. D. Paris, Claudia and L. Bruzzone, "A hierarchical approach to three-dimensional segmentation of lidar data at single-tree level in a multilayered forest," *IEEE Trans. Geosci. Remote Sens.*, vol. PP, no. 99, pp. 1–14, Jul. 2016.

[28] H. O. Ørka, E. Næsset, and O. M. Bollandsås, "Classifying species of individual trees by intensity and structure features derived from airborne laser scanner data," *Remote Sens. Environ.*, vol. 113, no. 6, pp. 1163–1174, Jun. 2009.

[29] M. Dalponte, H. O. Ørka, L. T. Ene, T. Gobakken, and E. Næsset, "Tree crown delineation and tree species classification in boreal forests using hyperspectral and als data," *Remote Sens. Environ.*, vol. 140, pp. 306–317, Jan. 2014.

[30] C. Zhang and F. Qiu, "Mapping individual tree species in an urban forest using airborne lidar data and hyperspectral imagery," *Photogramm. Eng. Remote Sens.*, vol. 78, no. 10, pp. 1079–1087, Oct. 2012.

[31] T. Brandtberg, "Individual tree-based species classification in high spatial resolution aerial images of forests using fuzzy sets," *Fuzzy Sets Syst.*, vol. 132, no. 3, pp. 371–387, Dec. 2002.

[32] J. Bohlin, H. Olsson, K. Olofsson, and J. Wallerman, "Tree species discrimination by aid of template matching applied to digital air photos," in *International Workshop 3D Remote Sensing in Forestry Proceedings*. University of Natural Resources and Applied Life Sciences (BOKU) Vienna, Feb. 14-15, 2006, pp. 199–203.

[33] M. Torma, "Estimation of tree species proportions of forest st ands using laser scanning," *Int. Arch. Photogramm. Remote Sens.*, vol. 33, no. B7/4; PART 7, pp. 1524–1531, Jul. 2000.

[34] X. Liang, J. Hyyppä, and L. Matikainen, "Deciduous-coniferous tree classification using difference between first and last pulse laser signatures," *International Archives of Photogrammetry, Remote Sensing and Spatial Information Sciences*, vol. 36, no. 3/W52, Sep. 2007.

[35] J. Holmgren and Å. Persson, "Identifying species of individual trees using airborne laser scanner," *Remote Sens. Environ.*, vol. 90, no. 4, pp. 415–423, Apr. 2004.

[36] S. Kim, "Individual tree species identification using lidar-derived crown structures and intensity data," Ph.D. dissertation, University of Washington, Seattle, WA, USA, 2007.

[37] Å. Persson, J. Holmgren, U. Söderman, and H. Olsson, "Tree species classification of individual trees in sweden by combining high resolution laser data with high resolution near-infrared digital images," *International Archives of Photogrammetry, Remote Sensing and Spatial Information Sciences*, vol. 36, no. 8, pp. 204–207, Oct. 2004.

[38] S.-R. Kim, W.-K. Lee, D.-A. Kwak, G. S. Biging, P. Gong, J.-H. Lee, and H.-K. Cho, "Forest cover classification by optimal segmentation of high resolution satellite imagery," *Sensors*, vol. 11, no. 2, pp. 1943–1958, Feb. 2011.

[39] R. Sugumaran and M. Voss, "Object-oriented classification of lidar-fused hyperspectral imagery for tree species identification in an urban environment," in *Urban Remote Sensing Joint Event, 2007*. IEEE, Apr. 2007, pp. 1–6.

[40] T. G. Jones, N. C. Coops, and T. Sharma, "Assessing the utility of airborne hyperspectral and lidar data for species distribution mapping in the coastal pacific northwest, canada," *Remote Sens. Environ.*, vol. 114, no. 12, pp. 2841–2852, Dec. 2010.

[41] S. Gupta, B. Koch, and H. Weinacker, "Tree species detection using full waveform lidar data in a complex forest," in *Technical Commission VII Symposium–100 Years of ISPRS*. Vienna University of Technology: Vienna, Austria, Jul. 2010, pp. 249–254.

[42] A. B. Chan, N. Vasconcelos, and G. R. G. Lanckriet, "Direct convex relaxations of sparse svm," in *Proceedings of the 24th international conference on Machine learning*, Corvalis, Oregon, Jun. 20–24, 2007, pp. 145–153.

[43] V. N. Vapnik and V. Vapnik, *Statistical learning theory*. Wiley New York, 1998, vol. 1.

[44] M. Roggero, "Object segmentation with region growing and principal component analysis," *International Archives of Photogrammetry Remote Sensing and Spatial Information Sciences*, vol. 34, no. 3/A, pp. 289–294, Sep. 2002.

[45] R. C. Veltkamp, "Boundaries through scattered points of unknown density," *Graphical Models and Image Processing*, vol. 57, no. 6, pp. 441–452, Nov. 1995.

[46] H. S. Horn, *The adaptive geometry of trees*. Princeton University Press, 1971, vol. 3, Princeton.

[47] F. Morsdorf, E. Meier, B. Kötz, K. I. Itten, M. Dobbertin, and B. Allgöwer, "Lidar-based geometric reconstruction of boreal type forest stands at single tree level for forest and wildland fire management," *Remote Sens. Environ.*, vol. 92, no. 3, pp. 353–362, Aug. 2004.

[48] C. Alexander, "Delineating tree crowns from airborne laser scanning point cloud data using delaunay triangulation," *Int. J. Remote Sens.*, vol. 30, no. 14, pp. 3843–3848, Jul. 2009.

[49] M. W. McDaniel, T. Nishihata, C. A. Brooks, P. Salesses, and K. Iagnemma, "Terrain classification and identification of tree stems using ground-based lidar," *Journal of Field Robotics*, vol. 29, no. 6, pp. 891–910, Nov. 2012.

[50] C. Ko, T. K. Remmel, and G. Sohn, "Mapping tree genera using discrete lidar and geometric tree metrics," *Bosque*, vol. 33, no. 3, pp. 313–319, Jan. 2012.

[51] V. Vapnik, "The nature of statistical learning theory." Springer, 2000, New York, pp. 138–141.

[52] C.-W. Hsu and C.-J. Lin, "A comparison of methods for multiclass support vector machines," *IEEE transactions on Neural Networks*, vol. 13, no. 2, pp. 415–425, Mar. 2002.

[53] K. Zhang and D. Whitman, "Comparison of three algorithms for filtering airborne lidar data," *Photogramm. Eng. Remote Sens.*, vol. 71, no. 3, pp. 313–324, Mar. 2005.

[54] I. Guyon, J. Weston, S. Barnhill, and V. Vapnik, "Gene selection for cancer classification using support vector machines," *Machine learning*, vol. 46, no. 1-3, pp. 389–422, 2002.

[55] M. Grant and S. Boyd, "CVX: Matlab software for disciplined convex programming, version 2.1," http://cvxr.com/cvx, Mar. 2014.

[56] C.-W. Hsu, C.-C. Chang, C.-J. Lin *et al.*, "A practical guide to support vector classification, tech. rep." Taipei, Apr. 2003.

[57] C.-C. Chang and C.-J. Lin, "Libsvm: a library for support vector machines," *ACM Transactions on Intelligent Systems and Technology (TIST)*, vol. 2, no. 3, p. 27, 2011.

[58] M. Gönen and E. Alpaydın, "Multiple kernel learning algorithms," *Journal of Machine Learning Research*, vol. 12, no. Jul, pp. 2211–2268, 2011.